CORE
Metadata, citation and similar papers at core.ac.uk

東北大学機関リポジトリ
TOUR
Tohoku University Repository

Maximum accuracy evaluation scheme for wireless saw delay-line sensors

著者	田中　秀治
journal or publication title	IEEE Transactions on Ultrasonics, Ferroelectrics and Frequency Control
volume	55
number	7
page range	1640-1652
year	2008
URL	http://hdl.handle.net/10097/46544

doi: 10.1109/TUFFC.2008.840

Maximum Accuracy Evaluation Scheme for Wireless SAW Delay-Line Sensors

Jan H. Kuypers, *Member, IEEE*, Leonhard M. Reindl, *Member, IEEE*, Shuji Tanaka, *Member, IEEE*, and Masayoshi Esashi, *Member, IEEE*

***Abstract*—This paper describes an evaluation scheme that prevents phase ambiguity of surface acoustic wave (SAW) delay-line sensors. Although it is well-known that phase evaluation yields accuracies of 150∼1500 times higher than time-delay evaluation, the problem of phase ambiguity has prevented phase evaluation of sensors operating over a range larger than 2π. This paper addresses this unsolved problem with a complete strategy. Furthermore, the existence of an optimum choice of the relative reflector positions on the sensor is shown. The presented relations enable the design of maximum accuracy SAW delay-line sensors.**

I. Introduction

Surface acoustic wave (SAW) delay-line sensors feature passive wireless interrogation for remote sensing and identification. This wireless sensor technology enables flexible measurement, monitoring of moving objects, and measurement in hazardous environments. In addition, there is a great interest to apply this technology to radio-frequency identification (RFID) with integrated sensors such as thermometers and strain gauges. This type of SAW sensor, illustrated in Fig. 1, has the advantage of being passive and, therefore, free from the replacement of batteries, featuring a long lifetime and high reliability. In addition, the wireless interrogation of these passive sensors is possible in a range up to several meters, depending on the legal restrictions of the transmission power and antenna gain. This operating range is considerably larger compared to inductively-powered, integrated RF ID sensors using 13.56 MHz.

In previous studies, SAW-based sensors were applied to the measurement of temperature, force, pressure, strain, torque, mass loading, and electrical signals, as overviewed in [1], [2]. However, only a few publications have discussed the achievable accuracy of such sensors and their signal-to-noise-ratio (SNR) dependence [2]–[5].

In particular, for a wireless interrogation, the SNR depends on the antenna-to-sensor alignment, which is likely to change in practice due to obstructions between the antenna and the sensor and environmental noise levels. Therefore, it is important to in-situ monitor the SNR in order to estimate the sensor accuracy and take actions accordingly. Especially for safety-related monitoring, the confidence level of the measurement has to be high, having a low false alarm rate. For RF ID applications, the in-situ monitoring of the SNR guarantees the reliability of the identification of items and persons.

This paper presents an evaluation scheme to achieve the maximum accuracy and methodology to quickly assess the sensor accuracy. This paper is organized in three parts. Based on the work by Schuster *et al.* [3], we will first understand the SNR dependence of the time delay and phase accuracy. We introduce a practical algorithm to extract the time delay and phase information from the sensor's time response. This concept is extended to account for modifications necessary to prevent spectral leakage of multiple reflector responses. Next, the sensitivity and the problem of phase ambiguity are presented. This enables us to compare the accuracies of a phase-based evaluation and a time-delay based evaluation. The second part introduces a multistep evaluation scheme in order to prevent phase ambiguities. The final section discusses the dependence of the optimum time delay of a SAW delay-line sensor.

II. Fundamental Sensor Relations

A. Time Delay and Phase Evaluation

The principle of using SAW delay-line devices for sensing is based on evaluating changes in the time delay and phase of the designed reflector responses. The typical time and phase response of such a sensor are illustrated in Fig. 1. The time delays τ_1, τ_2, and τ_3 are evaluated by determining the exact peak position of the time response. The phase values φ_1, φ_2, and φ_3 are extracted from the phase of the complex time response at the previously determined time delays τ_1, τ_2, and τ_3.

B. Sensor Effect

The time delay and phase are affected by any change in the propagation velocity of the SAW, e.g., due to temperature, strain, stress, mass loading, etc., and physical deformation of the delay line itself, e.g., thermal expansion, elongation (strain along the propagation direction), etc. In general for an effect X, the resulting time delay can be written as:

Manuscript received August 20, 2007; accepted January 24, 2008. This work was supported in part by the Strategic Information and Communications R&D Promotion Programme (SCOPE) from the Ministry of General Affairs (062302002).

J. H. Kuypers, S. Tanaka, and M. Esashi are with the Department of Nanomechanics, Graduate School of Engineering, Tohoku University, Sendai, Japan (e-mail: jan@mems.mech.tohoku.ac.jp).

L. M. Reindl is with the Laboratory for Electrical Instrumentation, Department of Microsystems Engineering (IMTEK), University of Freiburg, Freiburg, Germany.

Digital Object Identifier 10.1109/TUFFC.2008.840

0885–3010/$25.00 © 2008 IEEE

Authorized licensed use limited to: TOHOKU UNIVERSITY. Downloaded on March 10,2010 at 02:17:30 EST from IEEE Xplore. Restrictions apply.

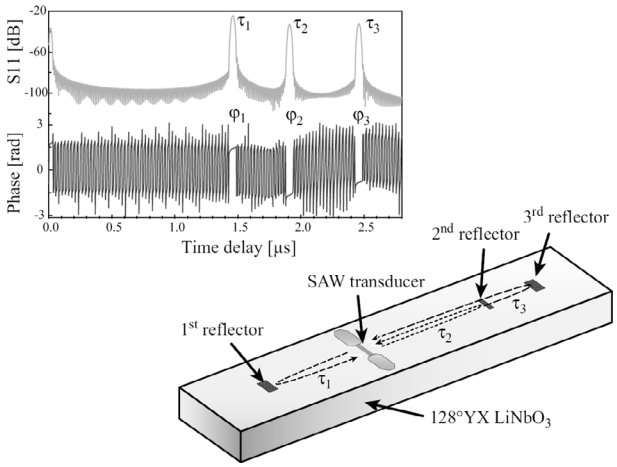

Fig. 1. SAW delay-line sensor having three reflectors in its acoustic track and corresponding simulated time delay and phase response [6], [7].

$$\tau(X) = \tau_0(1 + \mathrm{XCD} \cdot X), \tag{1}$$

where τ_0 refers to the initial time delay and XCD refers to the respective sensitivity coefficient of the delay toward the effect X. In case of temperature, the XCD is often referred to as TCD (temperature coefficient of time delay) or in the case of strain, as SCD (strain coefficient of time delay) [1].

For a dispersionless SAW delay-line sensor (i.e., a sensor without chirped interdigital transducer (IDT) or reflector structures [1]), the phase is related to the change in time delay via $\varphi = 2\pi f\tau$, where f refers to the operating frequency. The phase dependence, therefore, is given by:

$$\varphi(X) = 2\pi f\tau_0(1 + \mathrm{XCD} \cdot X). \tag{2}$$

For the sake of simplicity, we have assumed a linear sensor effect in (1) and (2). For the general case, the previous expression of the linear XCD is replaced by a series of:

$$\mathrm{XCD} \rightarrow \sum_{i=1}^{N} \mathrm{XCD}^i X^{i-1}. \tag{3}$$

Throughout this work we will be using the linear relations, given by (1) and (2), for the sake of clarity. However, the following theory and proposed evaluation method also is valid for nonlinear sensor effects as discussed in the final section.

C. Sensor Sensitivity

The sensitivity of the time delay toward a measurand X is found based on (1), as:

$$S_\tau = \frac{\partial\tau}{\partial X} = \tau_0\mathrm{XCD}. \tag{4}$$

Similarly, the sensitivity of the phase for the dispersionless, delay-line sensor is given by:

$$S_\varphi = \frac{\partial\varphi}{\partial X} = 2\pi f\tau_0\mathrm{XCD}. \tag{5}$$

D. Sensor Accuracy

For the practical application as a sensor, the measured time delay is related to the measurand X using the expression given in (1). This means that any uncertainty in the time-delay measurement (σ_τ) is related to uncertainty of X (σ_X), as:

$$\sigma_{X,\tau} = \frac{\sigma_\tau}{S_\tau}. \tag{6}$$

In the case of determining X based on a phase measurement, the uncertainty is given as:

$$\sigma_{X,\varphi} = \frac{\sigma_\varphi}{S_\varphi}. \tag{7}$$

We have assumed that the error during the time delay and phase measurement follows a normal distribution. We will see later that this assumed noise model of additive white Gaussian noise (WGN) is valid. In the case of stating the sensor accuracy, we will be referring to a value of $6\sigma_X$ in order to guarantee that the specified uncertainty accounts for 99.73% of the measurements.

The accuracies defined in (6) and (7) refer to the standard deviations of consecutive measurements, and not necessarily the absolute sensor accuracy. In order for (6) and (7) to correspond to the absolute sensor accuracy, any biasing effect caused by the overlap of reflector responses in the time domain must be prevented. This is achieved for the sensor design shown in Fig. 1 [6], [7] and the use of a suitable window function, as described in detail below. Furthermore, relating the deviations (6) and (7) to an absolute accuracy requires that we are able to perfectly describe the sensor characteristics over the measurement range. In general, calibration of each SAW sensor is necessary to obtain a best higher order fit of the sensor characteristics. However, as shown in [8] this fit is not able to account for higher order, nonlinearities inherent to each sensor. Therefore, a look-up table for each sensor is used to correct these nonlinear errors and to obtain the true value of the measurand. In this work we assume bias effects to be prevented due to the sensor design, the use of an appropriate window, and the knowledge of the exact sensor characteristic. In this case, measurement deviations relate to the absolute sensor accuracy.

III. Practical Measurement Accuracy

In the previous section we derived expressions of the resulting sensor accuracy. Although these expressions are of importance for the estimation of the sensor accuracy and the related design of such wireless sensors, the measurement accuracy itself is unknown. This section introduces the underlying theory that determines the measurement accuracy. Further practical considerations and an evaluation algorithm are presented. By comparing the results of applying this evaluation algorithm to a Monte Carlo simulation and actual measured data, the significance and validity of the proposed method are demonstrated.

Authorized licensed use limited to: TOHOKU UNIVERSITY. Downloaded on March 10,2010 at 02:17:30 EST from IEEE Xplore. Restrictions apply.

A. Wireless Sensor Interrogation

Advanced reader units for SAW-sensor interrogation are based on frequency-modulated or frequency-stepped continuous wave (FMCW/FSCW) radar technology [1]–[3]. The sampled output of the FMCW/FSCW unit contains the information of the sensor time delays and phase in the form of low-frequency, sinusoidal waves [3], as:

$$x[n] = \sum_{i=1}^{p} A_i \cos(2\pi\psi_i n + \varphi_i + \varphi_{\mathrm{ref},i}) + \upsilon[n], \qquad (8)$$

where p refers to the number of reflectors, A_i refers to the amplitude of the reflector response, ψ_i refers to the normalized frequency, φ_i refers to the phase of the reflector, $\varphi_{\mathrm{ref},i}$ refers to a phase offset, and $\upsilon[n]$ refers to additive white Gaussian noise, with zero mean and variance σ^2. Applying a discrete Fourier transform (DFT) to these data results in the typical time response of the sensor shown in the inset of Fig. 1. Besides the three main reflections, the radar output also contains sinusoidal waves due to environmental reflectors (radar clutter) and multiple reflector responses. By designing the time delays τ_1, τ_2, and τ_3 to be sufficiently large (i.e., larger than 1 μs [1]), the influence of environmental reflections is prevented. A technique to prevent influences between individual peaks is introduced later. For the moment we will assume that we are dealing only with one reflector. In this case, the radar output reduces to a single sinusoidal and additive white Gaussian noise.

B. Cramer Rao Lower Bound

The problem of extracting the frequency and phase information within white noise corresponds to a classic problem of estimation theory [9]. Based on this theory, the use of a maximum likelihood estimator enables these accuracies to approach the Cramer Rao Lower Bound (CRLB), which refers to the theoretical limit of the minimum uncertainties encountered in the measurement of time delay and phase. The CRLB of the measurement uncertainties of time delay and phase for a single reflector response for unknown frequency, amplitude, and phase are given by [3], [9] as:

$$\sigma_\tau(\eta) \approx \sqrt{\frac{12}{(2\pi)^2 \eta N B^2}}, \qquad (9)$$

and:

$$\sigma_\varphi(\eta) \approx \sqrt{\frac{2(2N-1)}{\eta N(N+1)}} \approx \sqrt{\frac{4}{\eta N}}, \qquad (10)$$

where N refers to number of samples, B refers to the measurement bandwidth covered by the frequency sweep of the radar, and η refers to the SNR defined as:

$$\eta = \frac{A_i^2}{2\sigma^2}. \qquad (11)$$

C. Simple Estimation Algorithm

The implementation of a wireless sensor system requires an evaluation algorithm to extract the time delay and phase information. Ideally, this algorithm should be as simple as possible, computation inexpensive, and should achieve the CRLB. The bounds for the computation expenses will depend on what hardware is used and in what time the evaluation has to be completed.

The method shown here uses an FFT (fast Fourier transform) with 16,384 samples per reading. The sample length of the 2.45 GHz FMCW Siemens SOFIS (Siemens AG, Braunschweig, Germany) reader used in this study is 1024 and is padded with zeros to the length of 16,384. The large zero padding is necessary to prevent the results from deviating from the CRLB due to uncertainties introduced by the discrete spacing (BINS) of the discrete Fourier transform, as discussed in [10].

The time delay is extracted by first performing a rough peak search on the DFT data $X[k]$, based on finding the maximum of the time response for a predefined time slot. The definition of this a-priori range is generally possible, as the peak positions in the time domain do not vary much due to the actual sensor effect. A shift of the time response due to a change in the read-out distance of a mobile sensor can be taken into account, but generally it is negligible. The rough estimate of the time delay is improved by fitting a second order polynomial through the maximum and its two closest neighbors, as used in [11] and solving for its maximum. The best estimate of τ for a three data point set of (a_i, b_i), where a_i refers to the time delay and b_i to the DFT result $|X[k]|$, is given as:

$$\hat{\tau} = \frac{a_1^2(b_2 - b_3) + a_2^2(b_3 - b_1) + a_3^2(b_1 - b_2)}{2(a_1(b_2 - b_3) + a_2(b_3 - b_1) + a_3(b_1 - b_2))}. \qquad (12)$$

These three points also are used to extract the phase of the reflector response. Here second order polynomials are fitted to both the real and imaginary parts of the complex time response and evaluated at the previously determined peak value $\hat{\tau}$. Based on normalizing the real $\hat{c}$ and imaginary part $\hat{d}$, the best estimate for the phase is found as:

$$\hat{\varphi} = \mathrm{Arg}\left(\frac{\hat{c}}{\sqrt{\hat{c}^2 + \hat{d}^2}} + j\frac{\hat{d}}{\sqrt{\hat{c}^2 + \hat{d}^2}}\right). \qquad (13)$$

D. De-Phasing

The discrete Fourier transform $X[k]$ generally is defined as:

$$X[k] = \sum_{n=0}^{N-1} x[n] \exp\left(-j\frac{2\pi}{N}kn\right). \qquad (14)$$

However, comparison with the integral definition of the Fourier transform shows that the summation should run from $-N/2$ to $(N/2) - 1$, as also discussed in [12]. This shift in the summation index corresponds to a time shift

Authorized licensed use limited to: TOHOKU UNIVERSITY. Downloaded on March 10,2010 at 02:17:30 EST from IEEE Xplore. Restrictions apply.

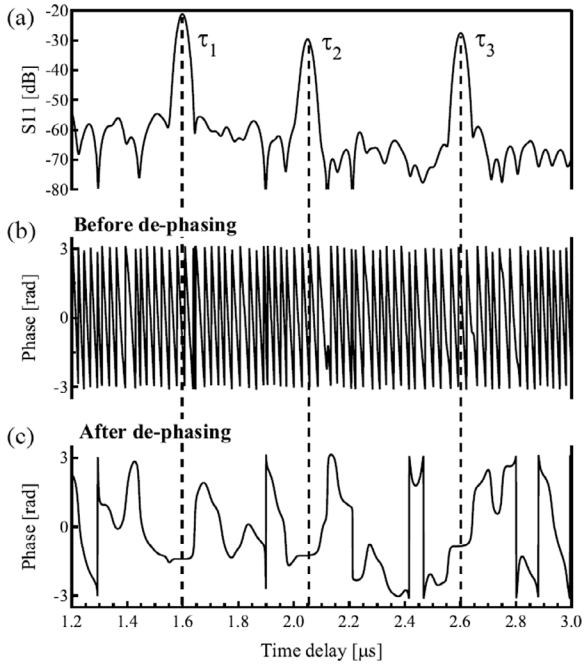

Fig. 2. Measured time response (a) for a wireless SAW sensor similar to [6], [7], having three reflectors as shown in Fig. 1. The phase for using a DFT implementation (14), starting with $n = 0$ is shown in (b). After de-phasing a flat phase in the region of the reflector responses is obtained (c), so that the phase uncertainty is now independent of uncertainties in the time delay estimation.

of the sampled data and leads to a fast rotation of the phase of the DFT output $X[k]$. The proposed phase estimation algorithm is largely influenced by this effect, as an uncertainty in the time delay estimation projected onto this slanted phase increases the phase uncertainty. This is seen from the measured time response of a sensor shown in Fig. 2(a), and the corresponding phase for the case without de-phasing shown in Fig. 2(b). The phasor is removed after DFT leading to the improved result $X_{DP}[k]$, according to:

$$X_{DP}[k] = X[k]e^{j2\pi i\frac{N}{2N_{\mathrm{FFT}}}} \quad i = 0, 1, \ldots, N_{\mathrm{FFT}} - 1, \tag{15}$$

where N corresponds to the sample length of the radar output (here 1024) and N_{FFT} corresponds to the length of the DFT result (here 16,384). This procedure is referred to throughout this paper as de-phasing. As seen from Fig. 2(c), the phase is now flat in the region of the reflector time delays, so that the phase estimation is independent of errors made during the preceding time-delay estimation. This simple procedure yields a reduction of the phase uncertainty of a factor of 2∼3, depending on the window function.

E. Performance Evaluation

A Monte Carlo simulation was carried out to verify the performance of the proposed evaluation algorithm in terms of the CRLB. The result of the time-delay accuracy is found to coincide with the theoretical limit given by (9). The obtained uncertainty of the phase is found to be one-half of the value suggested by (10), i.e., [3]. This originates from the fact that our evaluation algorithm makes use of the time-delay information to determine the phase. Therefore, the CRLB for the actual estimation problem is given as:

$$\sigma_\tau(\eta) \approx \sqrt{\frac{12}{(2\pi)^2\eta N B^2}}, \tag{16}$$

and:

$$\sigma_\varphi(\eta) \approx \sqrt{\frac{1}{\eta N}}, \tag{17}$$

respectively. Comparing the expression for the phase uncertainty of (17) using de-phasing to the result shown in (10), given by [3], shows that this simple method yields an improvement of factor two.

IV. Considerations for Multiple Reflectors

We have so far examined the measurement accuracy of time delay and phase for a given SNR value for a single reflector. However, the time delay and phase of the time response of a SAW delay-line sensor also depends on the distance between the reader antenna and the sensor. In practice, SAW delay-line sensors have at least two reflectors, as only the use of a relative time delay or phase of two reflectors ensures that the sensor distance has no effect on the sensor itself. Therefore, the actual estimation problem is concerned with the estimation of time delay and phase of multiple reflectors. The case of multiple sinusoidal signals with additive WGN, as given by (8), was first discussed by Rife and Boorstyn [13]. As shown in [13], the CRLB remains valid if the reflector positions are spaced far enough apart. In practice though, due to the spectral leakage during the DFT, the time delays are affected by the neighboring reflector responses, generally referred to as bias [12], [13]. This bias effect has to be prevented, and it is especially severe for a sensor system featuring parallel sensor interrogation with very closely spaced reflector responses of adjacent sensors, as presented in [6], [7]. In order to prevent the spectral leakage of reflector responses, a window function is applied to the sampled data prior to the DFT. However, as shown by Offelli and Petri [10], reduction of spectral leakage by applying a window function always increases the uncertainties of the estimator. This means that expressions (16) and (17) have to be modified to account for the effect of windowing. The minimum uncertainties obtainable for the case of windowing is referred to as modified CRLB (MCRLB) throughout this work.

A. Choice of Window Function

As mentioned earlier, for closely spaced reflector responses, spectral leakage effects are especially severe. In particular, for a multisensor system, the signal strength

Authorized licensed use limited to: TOHOKU UNIVERSITY. Downloaded on March 10,2010 at 02:17:30 EST from IEEE Xplore. Restrictions apply.

of individual sensors can vary considerably due to differences in operating range, alignment to the reader antenna or obstructions. Therefore, it is important to choose a window with very low sidelobe levels to prevent weaker signals from being affected by the bias caused by stronger reflector responses. We chose a minimum four-sample Blackman-Harris (BHM4S) window featuring a highest sidelobe level of −92 dB [12]. In the following we will discuss the effects of windowing and how the previously introduced expressions are adapted to account for these modifications.

B. Minimum Reflector Spacing

In order to prevent an overlap of adjacent reflector responses, a practical rule has been suggested by Schuster *et al.* [3]. It is based on using four times the value of the Rayleigh resolution limit as:

$$|\tau_p - \tau_q| > \frac{4}{B} \quad \text{for } p \neq q, \tag{18}$$

where τ_p and τ_q refer to the two adjacent reflector time responses and B refers to the bandwidth. As windowing causes a broadening of the peak width of the reflector responses in the time domain, this rule has to be increased by a factor of ∼2.13 for the BH4MS window. The factor of peak broadening is obtained by either analyzing the overlap of computed results or estimated based on the ratio of the 3 dB bandwidths of the rectangular window (0.89 bins) and the BH4MS window (1.9 bins). Applying this modified rule suppresses the spectral leakage below −95 dB.

C. Modified CRLB (MCRLB) Including Windowing

The effect of windowing concerning the CRLB has been discussed in literature by [10], [13]. For the case of sufficient zero padding, as in the case for our proposed algorithm, the effects of scalloping loss (i.e., the uncertainty caused by the time response coming to lie between two DFT points) becomes negligible. The combined effect of peak broadening and reduced SNR causes the time-delay inaccuracy for the BH4MS to increase by a factor of 2.16, obtained from Monte Carlo simulation. The variance of the phase is proportional to the inverse of the processing loss of the window, which is related to the scalloping loss (SL) and the equivalent noise bandwidth (ENBW), as shown by [10]. As in our case, the SL is prevented by sufficient zero padding, the increase in phase variance due to windowing is given by the ENBW of the window. As the ENBW is 2.00 for the minimum four-sample Blackman Harris window [12], the phase variance σ_φ^2 increases by a factor of two, and a factor of $\sqrt{2}$ in terms of σ_φ. The MCRLB for using the minimum four-sample Blackman Harris window thus can be stated as:

$$\sigma_\tau(\eta) \approx 2.16\sqrt{\frac{12}{(2\pi)^2 \eta N B^2}}, \tag{19}$$

and:

$$\sigma_\varphi(\eta) \approx \sqrt{\frac{2}{\eta N}}. \tag{20}$$

The phase uncertainty for the BH4MS window without de-phasing compared to the result derived in (20) is about 2.9 times larger. This is significantly larger than the factor of two previously obtained from comparing (17) and (10) for the case of no window.

D. Window Influence on the SNR Estimator

In the case of using a Monte Carlo simulation to analyze the performance of a given algorithm and window function, the SNR values are known. In practice, however, we will want our sensor system to estimate the SNR values of the reflectors based on the measurement data. By knowing the SNR values, the uncertainties of the time delay and phase are known so that the resulting sensor accuracy can be predicted based on (6) and (7).

The SNR for a sinusoidal signal had been defined in (11), based on the amplitude A_i of the signal and the variance of the WGN. The amplitude A_i is determined from the peak value of the DFT amplitude spectrum $|X[k_i]|$ as:

$$A_i = \frac{2|X[k_i]|}{N}, \tag{21}$$

where N corresponds to the sample length of the radar output. In the case of using a window, the amplitude of the reflector response in the DFT spectrum is reduced according to the coherent gain of the window, e.g., [12]. In the case of using the BHM4S window with a coherent gain of 0.36, the correct amplitude of the signal is given by:

$$A_i = \frac{2|X[k_i]|}{0.36 \cdot N}. \tag{22}$$

The variance of the WGN is estimated based on the DFT spectrum as suggested by [3]. This requires the use of a time slot without any reflector response, between k_a and k_b. The variance of the WGN then is given as:

$$\hat{\sigma}^2 = \frac{1}{N(k_b - k_a + 1)} \sum_{k=k_a}^{k_b} |X[k]|^2. \tag{23}$$

In the case of applying a window function, a correction factor has to be included. The factor was determined once again by performing a Monte Carlo simulation for given SNR values compared to the estimator result of (23). For the minimum four-sample Blackman Harris window, the expression of (23) has to be multiplied by a factor of ∼2.02 to yield a correct estimate of the SNR.

In the case of specifying the sensor accuracy based on the SNR estimation and the expression (19) and (20), it is important to verify the accuracy of the SNR estimator, which strongly depends on the width of the time slot. For $N = 1024$ and $B = 72$ MHz, a time slot of 200 ns yields an uncertainty of the SNR estimator of ∼5 dB (6σ), and a 400 ns time slot yields an accuracy of ∼3.5 dB (6σ).

Authorized licensed use limited to: TOHOKU UNIVERSITY. Downloaded on March 10,2010 at 02:17:30 EST from IEEE Xplore. Restrictions apply.

E. Combined Uncertainties

As previously mentioned, the sensor is based on using relative time delays and phase. For the sensor shown in Fig. 1, having three reflectors, the following time delay combinations are conceivable τ_{21}, τ_{31}, τ_{32} and analogue for the phase φ_{21}, φ_{31}, φ_{32}. For example the time delay τ_{21} corresponds to $\tau_2 - \tau_1$. This means that the uncertainty of τ_{21} both depend on the measurement uncertainty of τ_2 and of τ_1. In the case of independent errors, the combined uncertainty is given by:

$$\sigma_{\tau_{21}}(\eta_2, \eta_1) = \sqrt{\sigma_{\tau_2}(\eta_2)^2 + \sigma_{\tau_1}(\eta_1)^2}, \tag{24}$$

where we have assumed that the reflector strength and, therefore, the SNR of both reflector responses is not necessarily identical.

Based on the CRLB, we derive an expression for the effective SNR, which corresponds to the equivalent SNR for combined reflectors. By inserting the CRLB for the time delay (19) into (24), and solving for the effective SNR η_{21}, we get:

$$\eta_{21} = \left(\frac{1}{\eta_2} + \frac{1}{\eta_1}\right)^{-1}. \tag{25}$$

This means that, by computing the effective SNR for a time-delay combination based on (25), the relations of the CRLB can be applied directly. Inspection of the case for relative phase leads to the identical expression of (25).

In addition to the relative time delays and phase based on using two reflectors, we also will be using the relative time delay τ_{3221} and relative phase φ_{3221}. The time delay is thereby given by:

$$\tau_{3221} = \tau_{32} - \tau_{21} = \tau_3 - 2\tau_2 + \tau_1. \tag{26}$$

The resulting uncertainty for τ_{3221} has to take the repeated occurrence of τ_2 into account, as the repeated error is not independent. This leads to the combined measurement error of:

$$\sigma_{\tau_{3221}}(\eta_3, \eta_2, \eta_1) = \sqrt{\sigma_{\tau_3}(\eta_3)^2 + 4\sigma_{\tau_2}(\eta_2)^2 + \sigma_{\tau_1}(\eta_1)^2}. \tag{27}$$

Solving for the effective SNR, again based on the CRLB (19) for this combination, leads to:

$$\eta_{3221} = \left(\frac{1}{\eta_3} + \frac{4}{\eta_2} + \frac{1}{\eta_1}\right)^{-1}. \tag{28}$$

V. Results

In order to show the validity of the presented theory, the assumed noise model and the adaption to account for the effects of windowing, a Monte Carlo simulation as well as experimental data was analyzed.

A. Monte Carlo Simulation

The simulation was based on adding WGN to a sinusoidal signal, representing a single reflector, weighting this data with the BHM4S window, and applying our algorithm including the modified expressions, taking the windowing into account. The uncertainty of time delay and phase for a given SNR in the range of −25 to 25 dB was computed based on 2000 data sets per SNR. The result of the Monte Carlo simulation and the MCRLB given by (19) and (20) are shown in Fig. 3. The simulation agrees well with the predicted MCRLB for SNR values larger than −11 dB. Below this critical value of the SNR, often referred to as threshold [3], the accuracy predicted by the simulation strongly deviates from the MCRLB. As at these low SNR levels, the amplitude of noise starts to exceed the reflector peaks in the time domain, our rough peak search algorithm starts to fail in some cases. These detection errors cause the measurement accuracy to deviate strongly. As we will see later, SAW delay line sensors are operated well above the threshold SNR simply because the ambiguity is too large for any technical sensor application.

Based on the data from the Monte Carlo simulation for the uncertainty of a single reflector, using (24) and (25), the uncertainty for a relative time delay using two reflectors and three reflectors (τ_{3221}) based on (27) and (28), is estimated as well. As seen from Fig. 3, the use of the effective SNR makes all curves agree closely with each other and the MCRLB, except for the region below the threshold. It is important to point out that the threshold value depends on the number of reflectors, having its origin in the use of an effective SNR.

B. Experimental Results

In order to experimentally evaluate the measurement accuracy of time delay and phase, we used a 2.45 GHz FMCW Siemens SOFIS reader and fabricated 2.45 GHz SAW delay-line sensors having three reflectors, similar to the ones used in [6], [7]. In order to control the SNR during the measurement, we used a highly directive reader antenna mounted on a computer-controlled rotating pole. By misaligning the reader antenna and the SAW tag, the SNR could be controlled by a measurement program taking 100 data sets per 5° of rotation. Our algorithm was incorporated into the measurement program, including the SNR estimator.

As later done for the actual sensor, we examined the uncertainty of relative time delays i.e., τ_{21}, τ_{31}, τ_{32}, and τ_{3221}, and relative phase φ_{21}, φ_{31}, φ_{32}, and φ_{3221}. Computing the uncertainty of each data set versus the average effective SNR led to the results shown in Fig. 3. It can be seen that applying the definition of the effective SNR made all data points agree with each other. Furthermore, close agreement with the theoretical uncertainty given by the MCRLB and the Monte Carlo simulation was obtained. From the close agreement of the CRLB theory, extended to include windowing, with the results obtained from sim-

Authorized licensed use limited to: TOHOKU UNIVERSITY. Downloaded on March 10,2010 at 02:17:30 EST from IEEE Xplore. Restrictions apply.

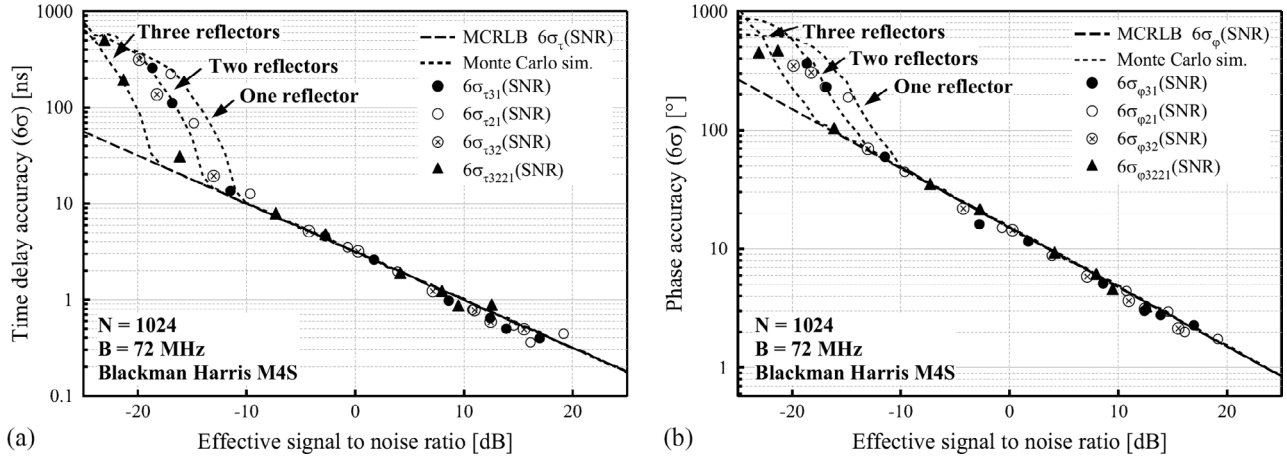

Fig. 3. Measurement accuracy of time delay (a) and phase (b) versus the SNR. The simulation is based on 2000 data sets per SNR, and the measured values are based on 100 data sets per SNR.

ulation and experiments, we confirm the validity of the given expressions and the proposed evaluation algorithm.

VI. Multistep Evaluation Scheme

After having confirmed the fundamental relations of the measurement accuracy based on the MCRLB, we are now able to compare the practical sensor accuracy based on a time delay and phase measurement given by (6) and (7), and the MCRLB for the minimum four-sample Blackman-Harris window of (19) and (20).

A. Sensor Accuracy: Phase-Based Evaluation versus Time-Delay Evaluation

We define this accuracy ratio, similar to [3], as a figure of merit (FOM) of using a phase-based evaluation over a time-delay based evaluation as:

$$\mathrm{FOM} = \frac{\sigma_{X,\varphi}}{\sigma_{X,\tau}} = 2\pi f \frac{\sigma_\tau}{\sigma_\varphi} = 2\pi f \frac{2.16\sqrt{\dfrac{12}{(2\pi)^2 \eta N B^2}}}{\sqrt{\dfrac{2}{\eta N}}} \approx \frac{4.32}{\sqrt{2}} \frac{\sqrt{3} f}{B}. \quad (29)$$

The factor of $4.32/\sqrt{2}$ in (29) is characteristic for the Blackman-Harris window. For a practical sensor system operating in the 2.45 GHz ISM band with a relative available bandwidth (B/f) of about 3%, the FOM is about 175, which indicates that the phase-based evaluation improves the sensor accuracy by 175 times. For a sensor system at 433 MHz and a B/f ratio as small as 0.4%, the FOM is as large as 1320. This explains why the phase evaluation of SAW sensors is attractive, as it achieves a much higher accuracy, especially for narrow band applications.

B. Phase Ambiguity

If a phase change of 2π does not cover the full measurement range, one measured phase corresponds to multiple values of X. Therefore, it is difficult to determine the actual value of X just using the phase. This problem of the phase-based evaluation is referred to as phase ambiguity. The phase ambiguity has been encountered in [11] and [14]. The first group has suggested that this problem can be overcome by mathematically weighting two relative phases to create an insensitive phase, e.g., as $\tau_{\mathrm{new}} = \tau_{31} - 2\tau_{21}$. This technique has been referred to by [3] as a solution to the phase ambiguity problem.

Possible weighting factors for this method are only integers. This means that the phase becomes more sensitive and, therefore, also the uncertainty increases by the same factor. In the example above the uncertainty increases by a factor of 1.53 ($\sqrt{14}/\sqrt{6}$) compared to the uncertainty of using $\tau_{\mathrm{new}'} = \tau_{31} - \tau_{21}$. This increased uncertainty reduces the operating SNR limit for the sensor, as seen later. We propose a multistep evaluation scheme, which is partly based on the idea of a stepwise method of the above mentioned approach, but without the use of mathematical weighting.

Reindl *et al.* [1] also mention the problem of phase ambiguity. They state that the number of reflectors necessary to prevent phase ambiguity increases with the measurement range. In our scheme, phase ambiguities can be prevented by using three reflectors, irrespective of the measurement range. We intend to clarify how to overcome the phase ambiguity with this work. In the next section, we present the design rules of a combined evaluation scheme to prevent phase ambiguity and to achieve a maximum sensor accuracy using the phase-based evaluation.

VII. Multistep Evaluation Scheme

We will first assume a sensor as shown in Fig. 4 with two reflectors corresponding to the time delays τ_1 and τ_2.

Authorized licensed use limited to: TOHOKU UNIVERSITY. Downloaded on March 10,2010 at 02:17:30 EST from IEEE Xplore. Restrictions apply.

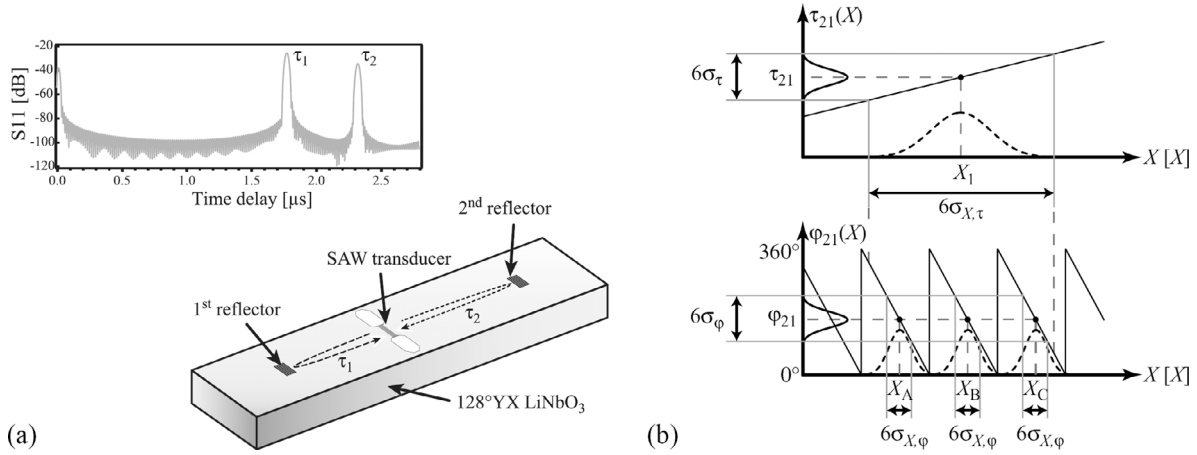

Fig. 4. SAW delay line sensor with two reflectors. (a) Layout of sensor. (b) Relative time delay and phase for a sensor sensitive to a measurand X, illustrating the effect of phase ambiguity.

As the absolute value of time delay and phase depends on the distance between sensor and antenna, length of cables, etc., relative time delay and phase values must be used, as e.g., $\tau_{21} = \tau_2 - \tau_1$. This also means that a one-reflector sensor is impractical, except for a distance, position, or velocity measurement.

A. Two-Reflector Configuration (τ_{21}, φ_{21})

The best measurement estimate using a time-delay difference is based on using the longest available relative time delay, as understood from (6). For the case of only two reflectors, this corresponds to the only relative time delay, which is τ_{21}. At the same time, evaluation of the relative phase φ_{21} generally would offer a 150∼1500 times better estimate of the actual measurand as seen from (29). In order to first estimate the measurand X based on τ_{21}, then improve the accuracy of X by next evaluating the phase φ_{21}, requires that the initial estimate of X is good enough to prevent any phase ambiguity of φ_{21}. This restriction is illustrated in Fig. 4(b). As seen, the measurement accuracy of the time delay τ_{21} and thus the first estimate of X is not sufficient to distinguish between the possible solutions of the phase φ_{21}.

The statement of this first estimate of X using τ_{21}, being smaller than the phase ambiguity, is derived as follows. Phase ambiguity does not occur in an interval of:

$$\Delta X < \frac{2\pi}{S_{\varphi_{21}}}, \tag{30}$$

so that from (6), the initial uncertainty of X is found as:

$$6\sigma_{X,\tau_{21}} = \frac{6\sigma_{\tau_{21}}}{S_{\tau_{21}}}. \tag{31}$$

This first estimation $6\sigma_{\tau_{21}}$ must be smaller than ΔX, where we have chosen a confidence level of $\pm 3\sigma$ for this decision. The uncertainty $\sigma_{\tau_{21}}$ assuming identical SNR levels of both reflectors (24), can be found as:

$$\sigma_{\tau_{21}} = \sqrt{2}\sigma_{\tau}. \tag{32}$$

The condition of preventing phase ambiguity based on (30), (31), and the use of (4) and (5) can be stated as:

$$\sigma_{\tau} < \frac{1}{6\sqrt{2}f}. \tag{33}$$

Generally, (33) is not satisfied except in cases of measurements with very high SNR and very large absolute bandwidths, as seen from (19). Therefore, a two-reflector design only achieves a high accuracy for very large SNR levels that are difficult to achieve for a wireless interrogation. The problem of phase ambiguity for this design has been reported in previous works [11], [14]. The trivial solution to this problem would be to place the reflectors closer together, decreasing their sensitivity, so that over the whole intended measurement range the phase does not exceed a range of 2π. Obviously, by decreasing the sensitivity, the accuracy drops as well, so that no or little accuracy enhancement is gained by the phase-based evaluation.

B. Three-Reflector Configuration (τ_{31}, φ_{3221}, φ_{31})

To solve the above mentioned problem, a three-reflector configuration is effective, realizing both unlimited operating range and high accuracy. The structure of this SAW delay-line sensor corresponds to the case depicted in Fig. 1. As shown in Fig. 5, the initial estimate of X is based on evaluating the largest available time delay, in this case τ_{31}, because the best accuracy of the time-delay-based measurement is obtained using the longest available relative time delay, as understood from (6). In order to be able to switch to the phase-based evaluation, we choose the most insensitive phase available, belonging to the smallest relative time delay available, which is $\tau_{3221} = \tau_{32} - \tau_{21} = (\tau_3 - \tau_2) - (\tau_2 - \tau_1)$, as introduced earlier in (26). A small time delay also can be obtained using only two reflectors, which are placed very close together. As explained above, if the spacing is too small and the reflectors overlap in the time response, this will introduce a large error, so that the CRLB is not valid. Therefore, a combination of three

Authorized licensed use limited to: TOHOKU UNIVERSITY. Downloaded on March 10,2010 at 02:17:30 EST from IEEE Xplore. Restrictions apply.

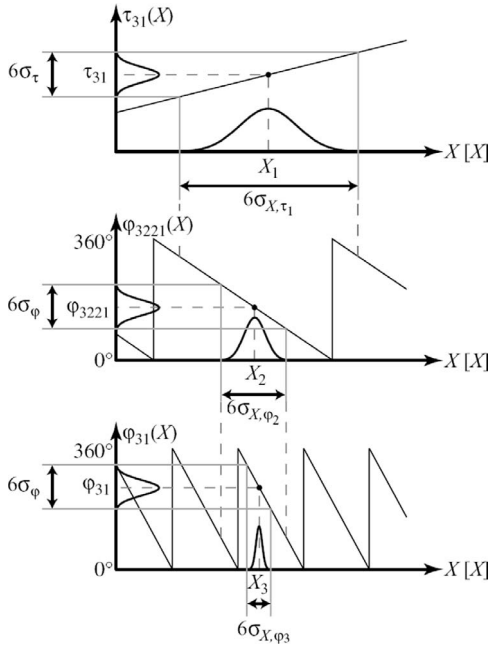

Fig. 5. Multistep evaluation scheme for a two-step transition ($\tau_{31} \rightarrow \varphi_{3221}$, $\varphi_{3221} \rightarrow \varphi_{31}$), based on combined time-delay and phase evaluations [6], [7].

reflectors is used instead, as suggested by [11]. Rewriting (33) for using φ_{3221}, we find:

$$\sigma_\tau < \frac{\tau_{31}}{\tau_{3221}} \cdot \frac{1}{6\sqrt{2}f}, \tag{34}$$

where we have made the assumption again that the SNR of reflectors 1 and 3 are identical. The result of (34) implies that the restriction of inequality (33) is weakened by a factor of τ_{31}/τ_{3221}. The final step is to evaluate the measurand at higher accuracy based on φ_{31}. Again, the uncertainty of φ_{3221} must be small enough to prevent the phase ambiguity for φ_{31}. Analogous calculations to (30) and (31) yield:

$$\frac{6\sigma_{\varphi_{3221}}}{\sigma_{\varphi_{3221}}} < \frac{2\pi}{S_{\varphi_{31}}}. \tag{35}$$

Solving for the critical uncertainty of phase φ_{3221}, and again assuming identical SNR ratios for all reflectors, we arrive at:

$$\sigma_\varphi < \frac{\tau_{3221}}{\tau_{31}} \cdot \frac{\pi}{3\sqrt{6}}. \tag{36}$$

Combining (34) and (36) yields:

$$\sigma_\tau \sigma_\varphi < \frac{\pi}{36\sqrt{3}f}, \tag{37}$$

which is the limiting inequality for the proposed multistep evaluation scheme, using first a time-delay measurement of τ_{31}, then a phase measurement of φ_{3221} and a final phase measurement of φ_{31}. Before examining some practical examples and the actual implication of using (37) instead of (33), we will look into one more possible scheme.

C. Advanced Three-Reflector Configuration (τ_{31}, φ_{3221}, φ_{21}, φ_{31})

So far we have discussed the scheme to avoid the phase-ambiguity problem by adding an intermediate step using the most insensitive phase, φ_{3221}. By this new scheme, the SNR restriction has been loosened drastically, as seen later in an example. Here, we propose an advanced scheme, which uses one more step, the evaluation of φ_{21}, to lower the critical SNR furthermore.

In the advanced scheme, the evaluation proceeds as $\tau_{31} \rightarrow \varphi_{3221}$, $\varphi_{3221} \rightarrow \varphi_{21}$, and $\varphi_{21} \rightarrow \varphi_{31}$. Without loss of generality, we choose the time delays as $\tau_{21} < \tau_{32}$. This means that τ_{21} is less sensitive than τ_{32}. This is rewritten using $\tau_{31} = \tau_{21} + \tau_{32}$, so that $\tau_{21} < \tau_{31}/2$, which means that φ_{21} is half or less sensitive than φ_{31}. Therefore, the critical SNR of the second step for $\varphi_{3221} \rightarrow \varphi_{21}$ is relaxed compared to $\varphi_{3221} \rightarrow \varphi_{31}$. The condition for avoiding the phase ambiguity in each step can be stated as (38), (39), and (40), respectively:

$$\frac{6\sigma_{\tau_{31}}}{S_{\tau_{31}}} < \frac{2\pi}{S_{\varphi_{3221}}}, \tag{38}$$

$$\frac{6\sigma_{\varphi_{3221}}}{S_{\varphi_{3221}}} < \frac{2\pi}{S_{\varphi_{21}}}, \tag{39}$$

$$\frac{6\sigma_{\varphi_{21}}}{S_{\varphi_{21}}} < \frac{2\pi}{S_{\varphi_{21}}}. \tag{40}$$

By rewriting (38), (39), and (40) in terms of the ratio τ_{31}/τ_{3221} and using $\tau_{21} = (\tau_{31} - \tau_{3221})/2$, we find two lower bounds for the ratio from (38) and (39), and one higher bound from (40), that is:

$$\max\left\{6\sqrt{2}\sigma_\tau f, \frac{\pi}{\pi - 6\sqrt{2}\sigma_\varphi}\right\} < \frac{\tau_{31}}{\tau_{3221}} < \frac{4\pi + 6\sqrt{6}\sigma_\varphi}{6\sqrt{6}\sigma_\varphi}. \tag{41}$$

Generally, the lower bound of τ_{31}/τ_{3221} is determined by the first term of (41). The minimum critical SNR η then is found by examining both cases as:

$$\sigma_\tau \sigma_\varphi < \frac{2\pi + 3\sqrt{6}\sigma_\varphi}{36\sqrt{3}f_0} \approx 2\frac{\pi}{36\sqrt{3}f_0}, \tag{42}$$

and:

$$\sigma_\varphi < \frac{\sqrt{1+\sqrt{3}} - 1}{3\sqrt{6}}\pi \approx 0.279122. \tag{43}$$

From comparing (42)[1] to the previous limiting case of (37), the restriction has been weakened by roughly a factor of two. From comparing the limiting value of η of (42) and (43), the minimum operating SNR is determined. As mentioned concerning (41), practically (42) is the limiting equation.

[1]Eq. (42) is a very rough approximation used only for the case of comparison with (37). For computation the full formula should be used for the sake of accuracy.

Authorized licensed use limited to: TOHOKU UNIVERSITY. Downloaded on March 10,2010 at 02:17:30 EST from IEEE Xplore. Restrictions apply.

TABLE I
EXAMPLES OF DIFFERENT MULTISTEP EVALUATION SCHEMES.

Case	Ref. no.	Transitions	Limiting relation	Relative time-delay ratios		Critical SNR η		Final sensor accuracy $6\sigma_x[X]$ (XCD = 1 ppm)	
				No window[1]	BHM4S[2]	No window	BHM4S	No window	BHM4S
A	2	none	none	none		none		$6\sigma_X \approx 2030.5\frac{1}{\sqrt{\eta}}$[3]	$6\sigma_X \approx 4385.8\frac{1}{\sqrt{\eta}}$
B	2	$\tau_{21} \rightarrow \varphi_{21}$	$\sigma_\tau < \frac{1}{6\sqrt{2}f}$	none		24.6 or 13.9 dB	114.7 or 20.6 dB	$6\sigma_X \approx 17.27\frac{1}{\sqrt{\eta}}$[4]	$6\sigma_X \approx 24.43\frac{1}{\sqrt{\eta}}$
C	3	1. $\tau_{21} \rightarrow \varphi_{21}$ 2. $\varphi_{3221} \rightarrow \varphi_{31}$	$\sigma_\tau\sigma_\varphi < \frac{\pi}{36\sqrt{3}f}$	$\frac{\tau_{31}}{\tau_{3221}} \approx 8.24$	$\frac{\tau_{31}}{\tau_{3221}} \approx 10.18$	0.36 or -4.4 dB	1.11 or 0.44 dB	$6\sigma_X \approx 17.27\frac{1}{\sqrt{\eta}}$	$6\sigma_X \approx 24.43\frac{1}{\sqrt{\eta}}$
D	3	1. $\tau_{21} \rightarrow \varphi_{21}$ 2. $\varphi_{3221} \rightarrow \varphi_{21}$ 3. $\varphi_{21} \rightarrow \varphi_{31}$	$\sigma_\tau\sigma_\varphi < \frac{2\pi + 3\sqrt{6}\sigma_\varphi}{36\sqrt{3}f}$	$\frac{\tau_{31}}{\tau_{3221}} \approx 12.16$	$\frac{\tau_{31}}{\tau_{3221}} \approx 14.9$	0.166 or -7.8 dB	0.52 or -2.87 dB	$6\sigma_X \approx 17.27\frac{1}{\sqrt{\eta}}$	$6\sigma_X \approx 24.43\frac{1}{\sqrt{\eta}}$

[1]Refers to the case of using no window function prior to DFT and is shown for comparison and reference purpose. In practice, the spectral leakage of multiple reflector responses requires windowing.
[2]Refers to the case of using a minimum 4-sample Blackman-Harris window [12].
[3]The accuracy based on using only a time delay evaluation is given by: $6\sigma_X = (6\sqrt{2}\sigma_\tau)/(\tau_{21}XCD)$.
[4]The accuracy based on using a phase evaluation is given by: $6\sigma_X = (6\sqrt{2}\sigma_\varphi)/(2\pi f\tau_{21}XCD)$.

D. Examples

In order to better understand the actual advantage of using (41) compared to (33) and (37), some general examples will be given. We will assume a system with a sample length of $N = 1024$, a bandwidth of $B = 72$ MHz, and a center frequency of $f = 2442$ MHz. This system is identical to the reader unit used in the previous work [6], [7] and similar to one used in [11]. Based on the derived relations in the previous section, four examples have been computed for the following cases: evaluation using only one relative time delay between two reflectors; a combined time-delay-based and phase-based evaluation using two reflectors; the multistep evaluation using three reflectors based on τ_{31}, φ_{3221}, and φ_{31}; and the advanced multistep evaluation using three reflectors based on τ_{31}, φ_{3221}, φ_{21}, and φ_{31}. The results for the four cases are given in Table I.

Comparing the first and second cases, for the case of using no window prior to DFT, the accuracy is improved by 118 times using the phase-based evaluation. In the case of using the Blackman-Harris window, the phase-based evaluation leads to an improvement of 180 times compared to the time-delay evaluation. However, the phase-based evaluation of the second case requires a very large SNR in order to prevent phase ambiguities. This SNR must exceed 20.6 dB for the case of using the window. The two-transition ($\tau_{31} \rightarrow \varphi_{3221}$, $\varphi_{3221} \rightarrow \varphi_{31}$) multistep scheme of the third case using a sensor with three reflectors, reduces the SNR requirement by a factor of 104 times ($\sim$20.2 dB) compared to the second case. As the final accuracy only depends on the phase evaluation of the largest time delay, the accuracy of the second and third cases are identical. By including an additional evaluation of φ_{21} ($\tau_{31} \rightarrow \varphi_{3221}$, $\varphi_{3221} \rightarrow \varphi_{21}$, $\varphi_{21} \rightarrow \varphi_{31}$: the fourth case, the SNR requirement is reduced by a factor of 222 (23.5 dB) compared to the second case, and factor of 2.14 (3.4 dB) compared to the third case.

The column at the right end of Table I gives the achievable accuracy based on the most sensitive phase, corresponding to the longest time delay. This accuracy is only available if the measurement achieves the specified critical SNR value to avoid phase ambiguity. To get an idea of the achievable accuracy for a practical sensor, we consider a SAW sensor with time delay $\tau_{31} = 1$ μs and sensor coefficient of delay XCD = 1 ppm/[X]. The sensor accuracy is easily converted to an arbitrary sensor effect. In case of a temperature sensor with a temperature coefficient of time delay (TCD) of 72 ppm/K, the phase-based evaluation of the second, third, and fourth cases for the case of using a window leads to:

$$6\sigma_T \approx 0.34\frac{1}{\sqrt{\eta}}\,\mathrm{K}. \tag{44}$$

Assuming an SNR of -1.5 dB, the temperature accuracy for the fourth case is $\sim$0.4 K. For the second and third cases, however, the critical SNR for the phase ambiguity is not achieved, and only the time-delay evaluation with an accuracy of 61 K is valid. For an SNR of 10 dB, a temperature accuracy of 0.1 K is obtained for the third and fourth cases, whereas the two-reflector sensor in the second case still suffers from phase ambiguity. Not until the SNR exceeds 20.8 dB does the sensor in the second case achieve the same accuracy as the third and fourth cases, which is $\sim$0.03 K.

E. Practical SNR Considerations

The previous section assumed identical SNRs for each reflector response, leading to simple expressions and allowing for an easy comparison of the individual evaluation schemes. However, the SNRs are practically not identical for different reflectors. This is taken into account by using the specific values of η_1, η_2, and η_3 for reflectors 1, 2, and 3, respectively, and relating them to the effective SNR introduced in (25) and (28). The strength of the reflector responses depends on the sensor design, so that for a uniform noise distribution in the time domain, which is the case for WGN, the ratios of the SNRs are fixed. Therefore,

Authorized licensed use limited to: TOHOKU UNIVERSITY. Downloaded on March 10,2010 at 02:17:30 EST from IEEE Xplore. Restrictions apply.

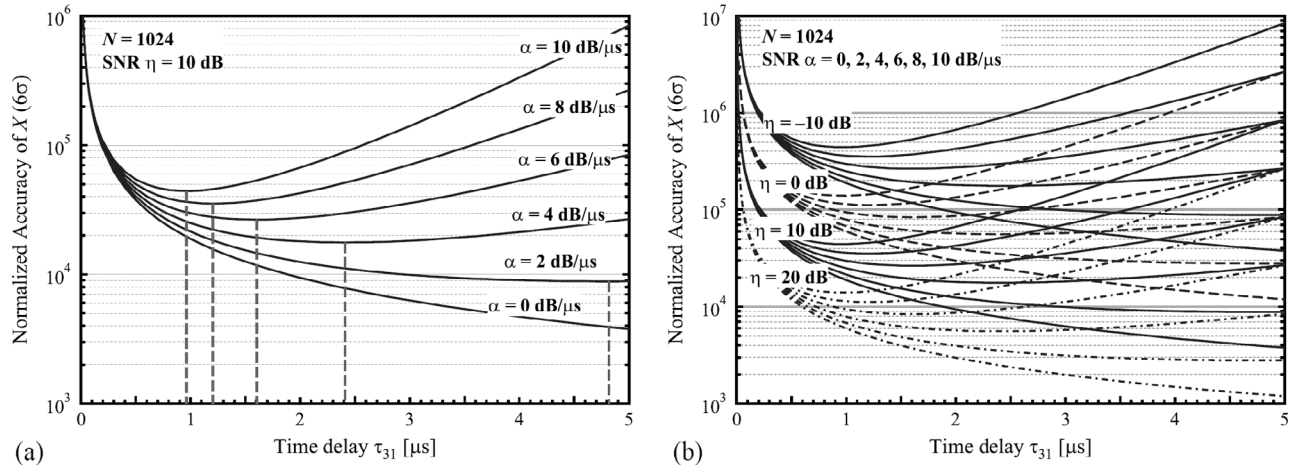

Fig. 6. Accuracy of measurand X determined by a phase evaluation of the largest relative time delay. Except for the ideal case of no propagation loss, an optimum value for the longest time delay exists. (a) Corresponds to the case of a constant SNR of 10 dB. (b) Shows that the optimum choice of τ_{31}, corresponding to the minimum of the uncertainty of X, is independent of the reflector SNR.

it often is helpful to define the SNRs relative to the SNR of reflector 1.

VIII. Optimum Reflector Delay

The sensor accuracy for a given time delay or phase had been derived earlier in (6) and (7), respectively. These relations in combination with (4) and (5) state that, by increasing the relative time delay the sensor accuracy improves. This also is seen from the examples shown in Table I in which the final accuracy depends on the largest time delay (here: τ_{21} or τ_{31}). However, by increasing the time delay, SAW propagation losses increase due to damping effects and diffraction losses. These losses increase rapidly, in particular for sensors operating at high frequencies, and reach 5∼6 dB/μs at 2.45 GHz [6]. Therefore, the question is how long the time delay should be to obtain a maximum sensor accuracy.

The answer is found based on the above relations of the CRLB. We consider the final accuracy of the measurand X based on the phase evaluation of τ_{31}. Assuming that τ_1 is constant, we now will investigate the influence of τ_3 on the overall measurement accuracy of X. In this case, instead of $\eta_1 = \eta_3$, we take:

$$\eta_3 = \eta_1 - (\tau_{31}\alpha) \text{ in [dB]}, \tag{45}$$

where α corresponds to the coefficient of propagation loss in dB/s, which includes the effect of diffraction by a linear approximation. The accuracy of measurand X for the case of the Blackman-Harris window is then found as:

$$\begin{aligned} 6\sigma(X) &= \frac{6\sqrt{\sigma_\varphi(\eta_1)^2 + \sigma_\varphi(\eta_3)^2}}{2\pi f XCD\tau_{31}} \\ &= \frac{6\sqrt{\frac{2}{N}}\sqrt{10^{-\frac{\eta_1}{10}}\left(1 + 10^{-\frac{\alpha\tau_{31}}{10}}\right)}}{2\pi(fXCD)\tau_{31}}, \end{aligned} \tag{46}$$

where η_1 and α are given in [dB] and [dB/s], respectively. In order to estimate the accuracy for a different window function, the factor of $\sqrt{2}$ has to be replaced by the appropriate value for the new window function, identical to the procedure leading to (20) earlier on. Fig. 6 illustrates the accuracy resulting from the phase-based evaluation for a given relative time delay, τ_{31}. In order to remain as general as possible, the uncertainty of X given in (46) has been normalized by the factor of $(fXCD)$, so that for a given center frequency and coefficient of time delay for the measurand, the accuracy can be directly obtained from Fig. 6(a). The dependence of the normalized accuracy on the SNR is illustrated in Fig. 6(b). It can be seen that, except for the ideal case without propagation loss, there is an optimum value of τ_{31} to maximize the sensor accuracy.

The optimum τ_{31} can be determined from Fig. 6, and the accuracy is estimated for the determined relative time delay. For example, consider a sensor system operating at 2.45 GHz with $f_0 = 2442$ MHz and a SAW propagation loss of 6 dB/μs. From Fig. 6(a) we directly see that a time delay of 1.6 μs would be ideal. If we can achieve an SNR of 10 dB in the measurement, we obtain a normalized accuracy value of 2.65×10^4 from Fig. 6(b). If this sensor is applied to a strain measurement with a sensor effect of $XCD = 8$ ppm/$\mu\varepsilon$, we can obtain the sensor accuracy by dividing the normalized accuracy by the operating frequency times the XCD, so that the sensor accuracy will be about 1.36 $\mu\varepsilon$.

IX. Discussion

Based on the introduced relations, the accuracy of SAW delay-line sensors is readily computed. The approach has been kept general, so that it is applicable to a wide range of SAW materials and sensor effects. In this paper, the linearity of the sensor effect had been assumed for the sake of brevity of equations. Nonlinearity can be included us-

Authorized licensed use limited to: TOHOKU UNIVERSITY. Downloaded on March 10,2010 at 02:17:30 EST from IEEE Xplore. Restrictions apply.

ing the general expression given in (3), based on a power series for a nonlinear sensor effect. Deriving the limiting inequalities of (33), (37), and (41) for this general definition, reveals that the proposed method does not depend on the definition of the XCD and its character. This is also understood from (33), (37), and (41) simply being independent of the XCD. Nevertheless, the achievable accuracy is now a function of the measurand X, and it is not a constant as for a linear sensor effect.

In addition, it should be pointed out that the proposed evaluation scheme is independent of the measurement range. This means that the proposed three-reflector design of a SAW sensor can cover an infinite measurement range. This is because the first evaluation step is based on a time-delay measurement, which does not suffer ambiguity no matter how large the measurement range is. With this we intend to clarify the misleading statement that the number of reflectors scales with increasing measurement range [1].

For a sensor system featuring in-situ estimation of the sensor accuracy, it is important to verify not only the validity of the MCRLB, including the effects of windowing, but also the accuracy of the SNR estimator. As discussed earlier concerning the SNR estimator given in (23), the accuracy depends strongly on the width of the time slot used for the SNR estimation.

X. Conclusions

This paper discusses the accuracy limitations of wireless SAW delay line sensors. An evaluation scheme that prevents phase ambiguity and allows for highest sensor accuracy using a final evaluation of the phase was presented. Based on the CRLB, the limiting accuracies for time delay and phase estimation were demonstrated, and practical relations for the estimation of the sensor accuracy were derived. These relations are of importance for the sensor design as well as the in-situ evaluation of the sensor accuracy during measurement based on the SNR.

We presented a simple evaluation algorithm for the time delay and phase evaluation of SAW delay-line sensors and demonstrated that it achieved the limiting uncertainty bound given by the CRLB. The necessity of using a window function prior to DFT to prevent spectral leakage of reflector responses was explained. In addition, we showed how windowing affects the CRLB, as well as how the SNR is estimated from the time response after windowing. The results obtained from Monte Carlo simulation and experiments agree well with this modified CRLB.

It also was shown that an optimum choice for the largest relative time delay exists to maximize the sensor accuracy. This relation is of practical importance for the design of wireless sensor systems. The presented graphical solution allows for a quick estimation of both the ideal time delay and the final sensor accuracy.

References

[1] L. Reindl, G. Scholl, T. Ostertag, H. Scherr, U. Wolff, and F. Schmidt, "Theory and application of passive SAW radio transponders as sensors," *IEEE Trans. Ultrason., Ferroelect., Freq. Contr.*, vol. 45, no. 5, pp. 1281–1292, 1998.

[2] A. Pohl, "A review of wireless SAW sensors," *IEEE Trans. Ultrason., Ferroelect., Freq. Contr.*, no. 2, pp. 317–332, 2000.

[3] S. Schuster, S. Scheiblhofer, L. Reindl, and A. Stelzer, "Performance evaluation of algorithms for SAW-based temperature measurement," *IEEE Trans. Ultrason., Ferroelect., Freq. Contr.*, vol. 53, no. 6, pp. 1177–1185, 2006.

[4] Y. Shmaliy, O. Ibarra-Manzano, and R. Rojas-Laguna, "A statistical model of passive remote SAW sensing employing differential phase measurement," in *Proc. IEEE Ultrason. Symp.*, 2004, pp. 1537–1540.

[5] V. A. Kalinin, "Passive wireless strain and temperature sensors based on SAW devices," in *Proc. IEEE Radio Wirel. Conf.*, 2004, pp. 187–190.

[6] J. H. Kuypers, D. A. Eisele, L. M. Reindl, S. Tanaka, and M. Esashi, "Passive 2.45 GHz TDMA based multi-sensor wireless temperature monitoring system: Results and design considerations," in *Proc. IEEE Ultrason. Symp.*, 2006, pp. 1453–1458.

[7] J. H. Kuypers, D. A. Eisele, L. M. Reindl, S. Tanaka, and M. Esashi, "2.45 GHz passive wireless temperature monitoring system featuring parallel sensor interrogation and resolution evaluation," in *Proc. IEEE Sensors*, 2006, pp. 773–776.

[8] R. Fachberger, G. Bruckner, R. Hauser, and L. Reindl, "Wireless SAW based high-temperature measurement systems," in *Proc. IEEE Freq. Contr. Symp.*, 2006, pp. 358–367.

[9] S. M. Kay, *Fundamentals of Statistical Signal Processing: Estimation Theory*. Englewood Cliffs, NJ: Prentice-Hall, 1993.

[10] C. Offelli and D. Petri, "The influence of windowing on the accuracy of multifrequency signal parameter estimation," *IEEE Trans. Instrum. Meas.*, vol. 41, no. 2, pp. 256–261, 1992.

[11] L. M. Reindl and I. M. Shrena, "Wireless measurement of temperature using surface acoustic wave sensors," *IEEE Trans. Ultrason., Ferroelect., Freq. Contr.*, vol. 51, no. 11, pp. 1457–1463, 2004.

[12] F. J. Harris, "On the use of windows for harmonic analysis with the discrete Fourier transform," *Proc. IEEE*, vol. 66, pp. 51–83, Jan. 1978.

[13] D. C. Rife and R. R. Boorstyn, "Multiple tone parameter estimation from discrete-time observations," *Bell Syst. Tech. J.*, vol. 55, pp. 1389–1410, 1976.

[14] X. Q. Bao, W. Burghard, V. V. Varadan, and K. V. Varadan, "SAW temperature sensor and remote reading system," in *Proc. IEEE Ultrason. Symp.*, 1987, pp. 583–585.

Jan H. Kuypers (M'05) received the Dipl.-Ing. degree from the Department of Microsystem Technology IMTEK at the University of Freiburg, Freiburg, Germany, in 2004, and the Ph.D. degree in Nanomechanics from Tohoku University, Sendai, Japan, in 2007. He has been working on the evaluation of mechanical properties of micromechanical systems (MEMS) thin films, deposition of aluminum nitride thin films, thin film bulk acoustic resonators, surface mounted resonators, modeling of surface acoustic wave (SAW) devices, wireless SAW sensors, MEMS-based SAW devices, and wafer level packaging. He is the author of the K-model, a higher order Green's function based simulation model for SAW devices.

He was awarded the best Student Paper at the IEEE Ultrasonics Symposium in 2007. He is currently working as a research specialist at the Berkeley Sensor and Actuator Center (BSAC) at the University of California, Berkeley, CA.

Authorized licensed use limited to: TOHOKU UNIVERSITY. Downloaded on March 10,2010 at 02:17:30 EST from IEEE Xplore. Restrictions apply.

Leonhard Reindl (M'93) received the Dipl. Phys. degree from the Technical University of Munich, Munich, Germany, in 1985 and the Dr. Sc. Techn. degree from the University of Technology Vienna, Austria, in 1997. From 1985 to 1999 he was a member of the micro acoustics group of the Siemens Corporate Technology Department, Munich, Germany, where he was engaged in research and development on surface acoustic wave (SAW) convolvers, dispersive and tapped delay lines, ID-tags, and wireless passive SAW sensors. In winter 1998–1999 and in summer 2000 he was guest professor for spread spectrum technologies and sensor techniques at the University of Linz, Linz, Austria. From 1999–2003 he was university lecturer for communication and microwave techniques at the Institute of Electrical Information Technology, Clausthal University of Technology, Clausthal. In May 2003 he accepted a full professor position at the laboratory for electrical instrumentation at the Institute for Micro System Technology (IMTEK), Albert-Ludwigs-University of Freiburg.

His research interests include wireless sensor and identification systems, SAW devices and materials as well as microwave communication systems based on SAW devices. He holds 35 patents on SAW devices and wireless passive sensor systems. He has authored/coauthored approximately 130 papers in this field. He is AdCommember of the IEEE Ultrasonics, Ferroelectrics, and Frequency Control Society and a member of the Microwave Theory and Techniques Society. Since 2000 he has been a member of the Technical Program Committee of the IEEE Frequency Control Symposium. He also is engaged in technical committees of the German Electrical, Electronic, and Information Technologies and Information Technology Society (VDE/ITG).

Shuji Tanaka received the B.E., M.E., and Dr.E. degrees all in mechanical engineering from the University of Tokyo in 1994, 1996, and 1999, respectively. From 1996 to 1999, he was a Research Fellow of the Japan Society for the Promotion of Science. He was a research associate at Department of Mechatronics and Precision Engineering, Tohoku University, Sendai, Japan, from 1999 to 2001, assistant professor from 2001 to 2003, and he is currently an associate professor at the Department of Nanomechanics. He was also a Fellow of the Center for Research and Development Strategy, Japan Science and Technology Agency, Tokyo, Japan, from 2004 to 2006, and is currently a Selected Fellow.

He was awarded the International Microprocesses and Nanotechnology Conference '98 Award for Outstanding Paper in 1999, and the Research Promotion Award from Miyagi Industrial Science Promotion Fund in 2007. His research interests include Power micromechanical systems (MEMS), RF MEMS, MEMS for harsh environments, and miniaturized gas turbine generators.

Masayoshi Esashi (M'89) was born in Sendai, Japan, on January 30, 1949. He received the B.E. degree in electronic engineering in 1971 and the Doctor of Engineering degree in 1976 at Tohoku University, Sendai, Japan.

From 1976 to 1981, he served as a research associate at the Department of Electronic Engineering, Tohoku University, and he was an associate professor from 1981 to 1990. He was a professor in the Department of Mechatronics and Precision Engineering there from 1990 to 1998. He was a Professor at the New Industry Creation Hatchery Center (NICHe) in Tohoku University from 1998 to 2005. Since 2005, he has been a professor at the Department of Nanomechanics, Graduate School of Engineering, Tohoku University. He was a Director of the Venture Business Laboratory in Tohoku University from 1995–1998. He is an associate director of the Semiconductor Research Institute, Sendai, Japan. He was a President of the Sensor-Micromachine Society in the Institute of Electrical Engineers in Japan (2002–2003). He has been a collaboration coordinator for Sendai City since 2004. He has been studying microsensors and integrated micro systems fabricated with micromachining.

Dr. Esashi served as a General Co-Chairman of the 4th IEEE Micro Electro Mechanical Workshop in 1991 held in Nara, Japan, and as a General Chairman of the 10th International Conference on Solid-State Sensors and Actuators (Transducers'99) in 1999 held in Sendai, Japan.

Authorized licensed use limited to: TOHOKU UNIVERSITY. Downloaded on March 10,2010 at 02:17:30 EST from IEEE Xplore. Restrictions apply.